ARTICLES

Journal of Semiconductors
(2023) 44, 122502
doi: 10.1088/1674-4926/44/12/122502

Hyperfine splitting and ferromagnetism in CdS : Mn nanoparticles for optoelectronic device applications

Madhavi Sharad Darekar† and Praveen Beekanahalli Mokshanatha

Department of Physics, Institute of Engineering and Technology, Srinivas University, Mukka, Surathkal, Mangalore-574146, Karnataka, India

Abstract: Manganese (Mn) doped cadmium sulphide (CdS) nanoparticles were synthesized using a chemical method. It was possible to decrease CdS : Mn particle size by increasing Mn concentration. Investigation techniques such as ultraviolet–visible (UV–Vis) absorption spectroscopy and photoluminescence (PL) spectroscopy were used to determine optical properties of CdS : Mn nanoparticles. Size quantization effect was observed in UV–Vis absorption spectra. Quantum efficiency for luminescence or the internal magnetic field strength was increased by doping CdS nanoparticles with Mn element. Orange emission was observed at wavelength ~630 nm due to $^4T_1 \rightarrow {}^6A_1$ transition. Isolated Mn^{2+} ions arranged in tetrahedral coordination are mainly responsible for luminescence. Luminescence quenching and the effect of Mn doping on hyperfine interactions in the case of CdS nanoparticles were also discussed. The corresponding weight percentage of Mn element actually incorporated in doping process was determined by atomic absorption spectroscopy (AAS). Crystallinity was checked and the average size of nanoparticles was estimated using the X-ray diffraction (XRD) technique. CdS : Mn nanoparticles show ferromagnetism at room temperature. Transmission electron microscopy (TEM) images show spherical clusters of various sizes and selected area electron diffraction (SAED) patterns show the polycrystalline nature of the clusters. The electronic states of diluted magnetic semiconductors (DMS) of Ⅱ–Ⅵ group CdS nanoparticles give them great potential for applications due to quantum confinement. In this study, experimental results and discussions on these aspects have been given.

Key words: synthesis; characterization; undoped CdS nanoparticles; Mn-doped CdS nanoparticles; non-aqueous chemical method

Citation: M S Darekar and P Beekanahalli Mokshanatha, Hyperfine splitting and ferromagnetism in CdS : Mn nanoparticles for optoelectronic device applications[J]. *J. Semicond.*, 2023, 44(12), 122502. https://doi.org/10.1088/1674-4926/44/12/122502

1. Introduction

Ⅱ–Ⅵ group compound semiconductors (e.g., CdSe, ZnS, CdS, etc.) are the most widely-used diluted magnetic semiconductors (DMS) and are doped with elements such as Gd, Tb, Eu, Co, Manganese (Mn), Fe, and so on. Due to the interaction between the spin induced magnetic moment of the transition metal ions and the charge carriers of the host semiconductor within the confined space of nanoparticles, the diluted magnetic semiconductors have interesting optical, electronic, and magnetic properties[1–3]. The efficient energy is transferred from the host materials to dopants due to the confinement of charge carriers in nanocrystals. Doped semiconductor nanoparticles can be used for display applications due to the efficient room temperature luminescence. These nanoparticles can be utilized for high density optical data storage applications due to the memory effect, for the fabrication of high efficiency solar cells, and so on. They can be applied in optoelectronics, spintronics, and rectifying diodes due to their novel luminescence and magnetic properties[2, 4].

Diluted magnetic semiconductors of type Ⅱ–Ⅵ are semiconductors in the bulk phase[5]. In this phase, host cations [Ⅱ] are randomly substituted by magnetic ions; Mn^{2+}. Ⅱ–Ⅵ group semiconductors show luminescence of isolated Mn^{2+} ions arranged in tetrahedral coordination at room temperature after adding a small amount of Mn^{2+} in this semiconductor. This luminescence is attributed to energy transfer from semiconductor to Mn^{2+} ions. However, its behavior depends on the method of preparation and also on concentration[6]. The diluted magnetic semiconductor behavior is confirmed by the room temperature ferromagnetism observed in CdS : Mn nanoparticles[4]. The electronic states of diluted magnetic semiconductor nanostructures give them great potential for applications due to the size quantization effect observed in them. Mn-doped CdS nanoparticles have been used for the fabrication of sensitized solar cell devices due to their enhanced power conversion efficiency. The traps for excited electrons obtained by CdS : Mn nanoparticles exhibit unique electronic, nonlinear, and optical properties[2].

Bulk CdS is a widely-used luminescent material[7]. Colloidal semiconductor quantum dots have been studied widely for their luminescence properties. Recent work on doped nanoparticles[8–17] shows that it is advantageous to use doped nanoparticles because they show increased quantum efficiency for luminescence. However, it is still necessary to investigate doped nanoparticles to understand them and also look for different applications. With this view, we have synthesized and investigated CdS nanoparticles doped with Mn.

Mn-doped CdS bulk material has been investigated[18]. The interest stems from the strong orange luminescence (λ_{em} = 585 nm) observed in this material. Mn doping at substitutional site in CdS, induces an acceptor state, which emits a bright orange luminescence with a peak at 2.12 eV (585 nm) due to $^4T_1 \rightarrow {}^6A_1$ transition which is shown in Fig. 1[19].

Correspondence to: M S Darekar, madhavi_darekar28@rediff.com
Received 4 JUNE 2023; Revised 27 JUNE 2023.

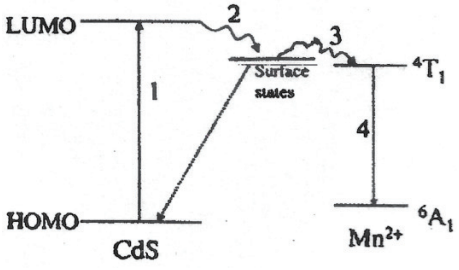

Fig. 1. Luminescence mechanism scheme of Mn-doped CdS nanoparticles[19].

McClure *et al*.[20] have used crystal field theory to understand the spectroscopic properties of *d*-electrons systems in transition metal ions. Mn^{2+} has $1s^2$, $2s^2$, $2p^6$, $3s^2$, $3p^6$, $3d^5$ electronic configurations. When Mn is placed in tetrahedral field of cubic CdS (from standard ASTM data), the transition from $^4T_1$ to $^6A_1$ occurs. The assignments of these transitions are presented in Tanabe–Sugano diagrams[21]. The strong luminescence band is attributed to Mn^{2+} emission in a tetrahedral coordination in $Cd_{1-x}Mn_xS$ (transition from $^4T_1$ to $^6A_1$) with photon energy of 2.12 eV. The intensity of the Mn^{2+} band increases with the increase in its concentration. The CdS band is not affected by the growth of the Mn/Cd ratio. This may exclude the possibility of energy transfer between Mn and Cd sites[22].

$Cd_{1-x}Mn_xS$ is a diluted magnetic semiconductor, where Cd is substituted by transition metal ion like Mn and *x* is the composition or concentration of Mn ions. The magnetic moment introduced due to magnetic ion in semiconductor gives rise to different interesting magnetic and magneto-optical properties, which are shown by the diluted magnetic semiconductors due to the exchange interaction of the band electrons with the magnetic ions. Unusual magneto-transport and magneto-optic phenomena, e.g., large Faraday rotation, giant negative magneto-resistance, and magnetic field induced metal–insulator transition, are observed due to the *sp*–*d* spin exchange interaction constituting a unique interplay magnetism[22].

It may be noted here that bulk CdS is usually doped by thermal diffusion at high temperature but, as shown by ourselves as well as Levy *et al*.[22], doping is possible even at room temperature. This may be a great advantage of nanoparticles doping. This group has shown the possibility of doping CdS particles of different sizes and different concentrations. In this work, an attempt is made to prepare CdS particles of approximately the same size by the variation in low concentrations of Mn element.

Mn-doped CdS nanocrystals were prepared by using methods like the colloidal chemistry method[23], chemical precipitation method[1, 24–29], air-stable single-source precursor[30], sol-gel method[7], novel hydrothermal method[31], chemical bath deposition method[32], and so on. These nanoparticles can be used in the fabrication of photovoltaic devices due to doping of the Mn element. Mn^{2+} ions produce some surface or defect sites for the excited electrons in case of Mn-doped CdS nanoparticles, which have potential applications in electronic devices, optoelectronic devices, and nonlinear optics[26].

In this study, Mn-doped CdS nanoparticles were synthesized with thioglycerol (T.G.) acting as the organic capping agent using the non-aqueous chemical method at room temperature by varying the concentration of Mn element. These doped nanoparticles were analyzed by using the investigation techniques such as ultraviolet–visible (UV–Vis) absorption spectroscopy, X-ray diffraction (XRD), photoluminescence (PL) spectroscopy, atomic absorption spectroscopy (AAS), electron spin resonance (ESR), vibrating sample magnetometry (VSM), and so on. For doping of Mn, manganese chloride ($MnCl_2$) was mixed in proper proportion to cadmium acetate. This allows us to control the concentration of dopant. In the case of Mn doping, 0.015 to 0.080 M of manganese chloride was added to cadmium acetate solution and the corresponding weight percentage of the Mn element that was actually incorporated in the doping process was determined by AAS.

The preparation of CdS : Mn nanoparticles using the non-aqueous chemical method at room temperature has not been reported earlier. The effects of the Mn composition on the magnetic and structural properties of CdS nanoparticles have been analyzed[26]. Due to their unique optical, electronic, structural, and magnetic properties, these doped nanoparticles have great potential in variety of applications.

2. Experimental

Mn-doped CdS nanoparticles have been synthesized by a very simple method at room temperature under nitrogen atmosphere. $MnCl_2$ was added to cadmium acetate [$Cd(CH_3COO)_2$] and a similar procedure was followed as that used to synthesize undoped CdS nanoparticles in our previous study[33]. Cadmium acetate taken in the reaction vessel was stirred using a magnetic stirrer. Manganese chloride, thioglycerol [$SHCH_2CH(OH)CH_2OH$], and sodium sulphide (Na_2S) were then added step by step into the solution through an equalizer and the whole solution was stirred continuously. Ethyl alcohol (C_2H_5OH) was used in solution preparations. Here it should be noted that in case of Mn-doped CdS nanoparticles, thioglycerol has been used as the additive and all the solution parameters have been kept unchanged. The amount of Mn weight percentage has been varied by changing the amount of manganese chloride mixed with cadmium acetate. After the reaction was completed, all thioglycerol stabilized CdS : Mn particles were washed with acetone and diethyl ether, and vacuum dried.

All the chemicals used in the experimental part were analytical reagent (A.R.) grade chemicals and they were used without further purification.

3. Results and discussion

Table 1 shows the properties of thioglycerol, which acts as the organic capping agent. A Schimadzu UV-300 double beam spectrometer was used for UV–Vis absorption studies. The UV–Vis absorption peak appears at 513 nm with an energy gap of 2.42 eV in bulk CdS material. Fig. 2 shows the UV–Vis absorption spectra of thioglycerol capped Mn-doped CdS nanoparticles with varying concentration of Mn element. The amount of Mn incorporated in particles ranges from 0.068 to 0.154 atomic wt.% (samples A to J), which is shown in Table 2.

From Fig. 2, it is observed that the UV–Vis absorption value has decreased with an increase in concentration of Mn

Table 1. Properties of thioglycerol.

Parameter	$SHCH_2CH(OH)CH_2OH$
Density	1.295 gm/mL
Molecular weight	108.16 gm/mole
Purity	99%
Molarity	11.9 M
Boiling point	118 °C
Freezing point	110 °C

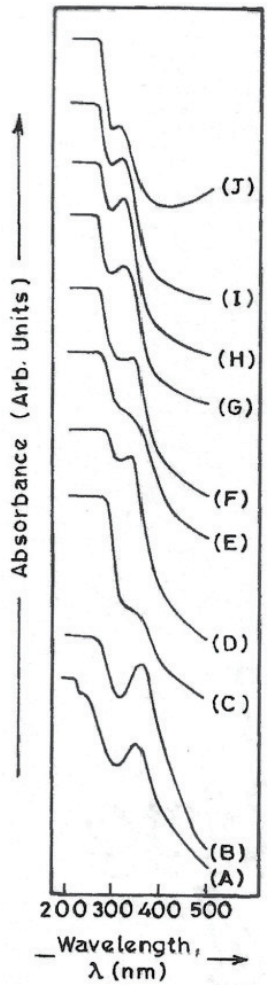

Fig. 2. UV–Vis absorption spectra of Mn-doped CdS nanoparticles (samples A to J).

element. This means that the particle size, as calculated by using the effective mass approximation[33], decreases and the energy gap, as found out by using the Planck's quantum theory of radiation[33–35], increases as the Mn composition increases. The equation of the energy of a photon, $E = h\nu$ was used to calculate the energy gap of the semiconductor nanoparticles. The radius of the cluster has been estimated by using the equation of the excited state energy ΔE,

$$\Delta E = \frac{\hbar^2\pi^2}{2R^2}\left[\frac{1}{m_e} + \frac{1}{m_h}\right] - \frac{1.8e^2}{\varepsilon R} + \text{polarization energy}. \quad (1)$$

As the polarization energy of the cluster or the solvation energy loss, is very small and size independent, it is neglected. The first and the second terms are the quantum energy of localization and the coulomb energy of electron–hole attraction, respectively. The values of the first

Table 2. UV–Vis absorption values, band gap values and particle sizes of Mn-doped CdS nanoparticles (samples A to J).

Sample	Wt.% of Mn used for chemical reaction	Wt.% of Mn found by AAS	At. Wt.% of Mn found by AAS	UV–Vis absorption (nm)	Band gap E_g (eV)	Particle size (nm)
A	15	3.72	0.068	358	3.46	5.28
B	25	4.56	0.083	365	3.40	5.36
C	35	5.66	0.103	350	3.54	5.18
D	45	6.48	0.118	340	3.65	5.06
E	50	6.87	0.125	336	3.69	5.02
F	55	7.20	0.131	330	3.76	4.95
G	60	7.53	0.137	318	3.90	4.81
H	65	7.80	0.142	315	3.94	4.78
I	70	8.02	0.146	310	4.00	4.73
J	80	8.46	0.154	300	4.14	4.61

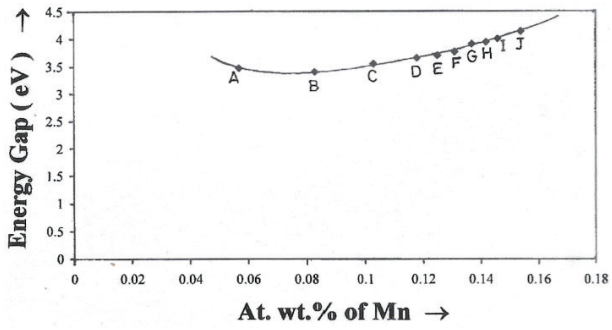

Fig. 3. Variation of energy gap with atomic weight percentage of Mn in Mn-doped CdS nanoparticles (samples A to J).

and the second terms increase as the cluster radius decreases and the signs of these two terms are opposite. This effectively means that there is an increase in the energy gap with a decrease in the particle size of the semiconductor material, which is seen in Table 2. The equation of the energy gap is given as

$$E = E_g + \Delta E, \quad (2)$$

where E_g is the energy gap of the bulk semiconductor material and ΔE is the exciton energy.

Fig. 3 shows the variation of energy gap with the atomic weight percentage of Mn element in Mn-doped CdS nanoparticles (samples A to J). Fig. 3 shows a decrease in the direct energy band gap up to 3.40 eV (sample B), and then the band gap energy increases up to 4.14 eV (sample J). This behavior is observed with an increase in the Mn concentration. From Fig. 3, it is clear that the band gap energy varies non-linearly with an increase in Mn concentration. Levy *et al.*[18, 22] have also shown the nonlinear variation of the energy band gap with the Mn composition with a well-noticeable minimum. The monotonic variation of the band gap energy with the Mn composition for the calculated particle size was not detected in the bulk phase of Mn-doped diluted magnetic semiconductors[25]. The appearance of the lowest point in the band gap energy with increasing Mn composition is attributed to a quantum size effect, and due to exchange interactions between Mn^{2+} *d* electrons and the conduction and valence band electrons in the bulk phase of CdS : Mn. The lowest point in the band gap energy will be

observed in CdS : Mn nanoparticles due to the increment in the exchange interactions between Mn^{2+} *d* electrons and the conduction and valence band electrons at the given temperature. A well-defined lowest point in the band gap energy (3.40 eV) with increasing Mn concentration is observed for CdS : Mn nanoparticles (sample B) having 5.36 nm particle size. This suggests that there is a significant increase in the exchange interactions between Mn^{2+} ion-band electrons in comparison with the bulk[25]. The UV–Vis absorption value, the band gap values, the particle sizes of samples A to J (having higher Mn concentrations) are given in Table 2. The nonlinear variation of the band gap with Mn composition is observed in samples A to J. Levy *et al*.[5] has shown the same behavior for a similar average particle size. For a given particle size, the band gap does not vary monotonously with Mn composition. The minimum in the band gap energy versus Mn composition is more pronounced and its depth increases with increasing the particle size. This behavior of the energy band gap depends on the concentration of Mn element and the particle size. Similar behavior was observed in the bulk phase[36] and films[37]. In the case of very small Mn-doped CdS nanoparticles having the average particle size of 1.8 nm, the well-defined lowest point in the energy gap versus the Mn concentration was observed due to the enhancement in the exchange interactions between the Mn^{2+} *d* electrons and the conduction and valence band electrons in comparison with the bulk[25]. The nonlinear variation of the energy gap with an increase in the Mn concentration indicates the presence of exchange interactions in our study. The values of the energy gaps found out from the UV–Vis absorption spectra of Mn-doped CdS nanoparticles synthesized by us are higher than that calculated by Stojic *et al*.[25]. The values of the weight percentage of the Mn element used in the synthesis of Mn-doped CdS nanoparticles by Stojic *et al*. are higher than those used in this study. This means that the particle size increases with increasing the Mn concentration in the case of CdS : Mn nanoparticles prepared by Stojic *et al*. The band gap energy does not vary monotonically with the Mn composition for the obtained particle size[25].

The values of the absorption wavelengths in the visible range of the UV–Vis absorption spectra of Mn-doped CdS nanoparticles prepared by Gadalla *et al*.[1], Costa *et al*.[38], Venkatesu *et al*.[29], and Hoffmann *et al*.[39] are higher than that observed in our study.

Levy *et al*.[5] have demonstrated that the use of colloidal assemblies permits to control independently the size and composition of $Cd_{1-y}Mn_yS$ nanosized particles, and Mn ions are substituted randomly in the CdS matrix. The appearance of the minimum in the energy band gap with increasing Mn composition could not be attributed to a chemical disorder but to a quantum size effect, and due to the exchange interactions of the conduction and valence band electrons with the Mn^{2+} *d* electrons[40].

Fig. 4 shows the UV–Vis absorption spectrum of Mn-doped CdS nanoparticles (sample K having 0.085 M of manganese chloride). From Fig. 4, it is clearly seen that the UV–Vis absorption peak is observed at the same wavelength ~290 nm (energy gap ~4.28 eV) with nearly the same sharpness as was observed in case of pure CdS nanoparticles (sample A)[35]. Even though the concentration of thioglycerol in pure CdS nanoparticles (sample A)[35] is higher than that in

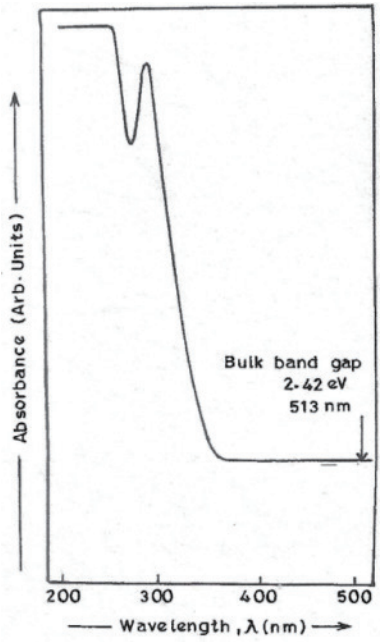

Fig. 4. UV–Vis absorption spectrum of Mn-doped CdS nanoparticles (sample K).

sample K, the UV–Vis absorption value remains almost the same in both cases. This means that the UV–Vis absorption value depends on the concentration of Mn element in case of CdS : Mn nanoparticles. In the case of bulk CdS semiconductor material, the UV–Vis absorption peak is observed at ~513 nm with an energy gap of ~2.42 eV. The monotonic variation of the band gap energy with the Mn concentration for the calculated particle size will not be observed in the bulk phase of Mn-doped diluted magnetic semiconductors[25].

Mn-doped CdS particles (samples R to Z) having low Mn concentration (shown in Table 3) have been synthesized, which showed the linear variation of the band gap with particle size as reported earlier[22]. Fig. 5 shows the UV–Vis absorption spectra of Mn-doped CdS nanoparticles doped from 0.0005 to 0.0671 atomic wt.% of Mn (samples R to Z). From Fig. 5, it is seen that there is a red shift in the absorption wavelengths with an increase in the Mn composition. Table 3 shows that the UV–Vis absorption value increases with an increase in the Mn concentration. This means that there is an increase in the particle size and a decrease in the band gap as the Mn composition increases. Thus, it is clear that the absorption spectrum of Mn-doped CdS nanoparticles is size dependent.

The size quantization effect is observed in samples R to Z. The Mn concentration has been shown by AAS studies. A Baird Atomic alfa–4 (UK) atomic absorption spectrophotometer was used for AAS studies. Fig. 6 shows the variation of energy gap with the particle size in Mn-doped CdS nanoparticles (samples R to Z). The size of the particles R to Z (having lower Mn concentration) falls in the narrow range of 3.76 to 4.46 nm. The size of the CdS : Mn nanoparticles (samples R to Z) has been found by using the effective mass approximation. From Fig. 6, it is clearly seen that there is a decrease in the band gap energy up to 3.35 eV (sample Z) with an increase in the particle size. From Fig. 6, it is observed that the band gap energy varies linearly with the particle size. The UV–Vis absorption values, the band gap values, the particle

Table 3. UV–Vis absorption values, band gap values and particle sizes of Mn-doped CdS nanoparticles (samples R to Z).

Sample	Wt.% of Mn used for chemical reaction	Wt.% of Mn found by AAS	At. Wt.% of Mn found by AAS	UV–Vis absorption (nm)	Band gap E_g (eV)	Particle size (nm)
R	6.4×10^{-5}	0.026 ± 0.002	0.0005	346	3.59	5.13
S	8×10^{-5}	0.078	0.0014	350	3.54	5.18
T	2×10^{-4}	0.132	0.0024	350	3.54	5.18
U	3×10^{-4}	0.152	0.0028	352	3.52	5.21
V	4×10^{-4}	0.24	0.0044	355	3.49	5.24
W	5×10^{-4}	0.3	0.0055	357	3.47	5.27
X	7×10^{-4}	0.62	0.0113	360	3.45	5.29
Y	1×10^{-3}	1.24	0.0226	366	3.39	5.37
Z	5×10^{-3}	3.72	0.0671	370	3.35	5.42

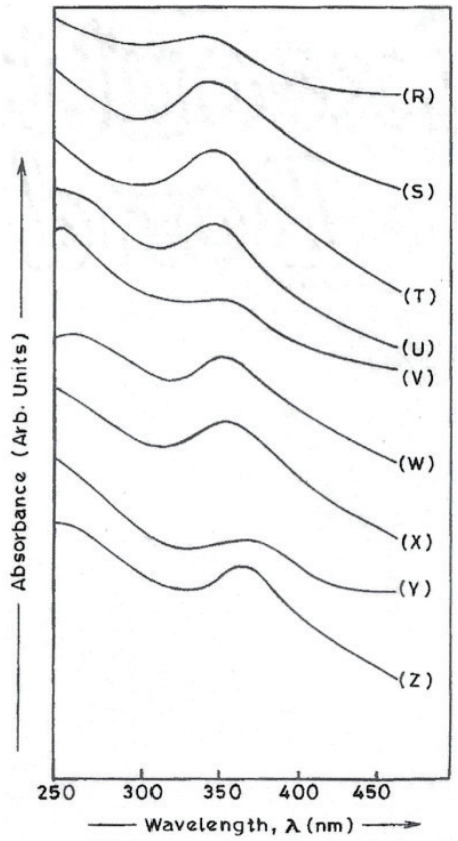

Fig. 5. UV–Vis absorption spectra of Mn-doped CdS nanoparticles (samples R to Z).

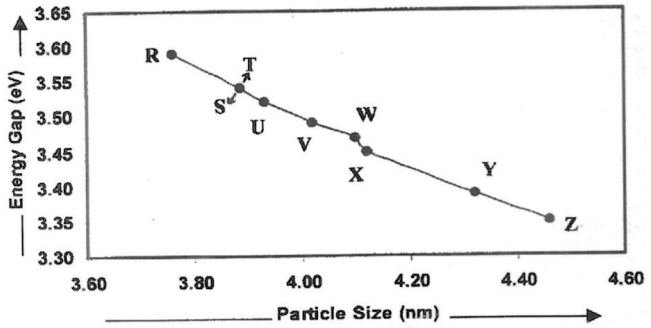

Fig. 6. Variation of energy gap with particle size in Mn-doped CdS nanoparticles (samples R to Z).

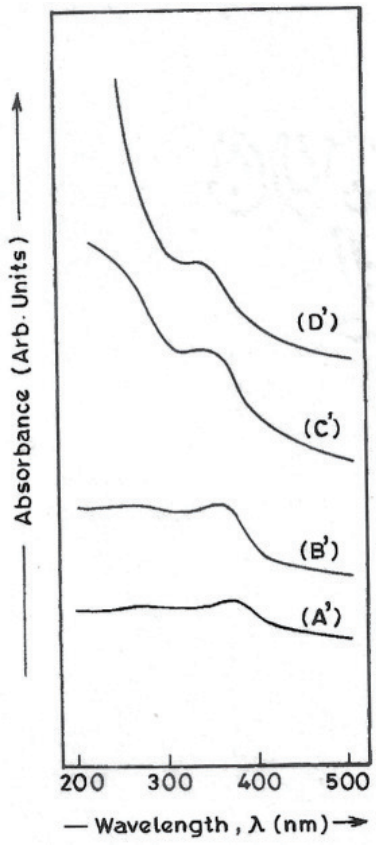

Fig. 7. UV–Vis absorption spectra of Mn-doped CdS nanoparticles (samples A′, B′, C′ and D′).

sizes of samples R to Z are given in Table 3. Thus, it is concluded that a linear variation of the band gap with the particle size is observed when the Mn concentration increases. Levy *et al*.[22] have demonstrated a red shift in the UV–Vis absorption values with increasing the Mn concentration, thus indicating the linear variation of the band gap with particle size. The sharp excitonic peaks are observed for very small sized direct semiconductor nanoparticles. This behavior is assigned to the quantum size effect[22].

The non-aqueous chemical method has also been used to obtain four more samples: A′, B′, C′ and D′ at room temperature. Fig. 7 shows the UV–Vis absorption spectra of the four samples A′, B′, C′ and D′. These spectra show the size quantization effect. Fig. 7 shows a blue-shift in the absorption spectrum with an increase in concentration of Mn element. The direct energy band gap deduced from the absorption spectrum increases with decreasing the UV–Vis absorption value. Since the UV–Vis absorption value depends on the particle size, there is a decrease in the particle size with increasing the Mn concentration. Table 4 shows the UV–Vis absorption values, the optical energy gap values, and the particle sizes of samples A′, B′, C′ and D′.

Table 4. UV–Vis absorption values, band gap values and particle sizes of Mn-doped CdS nanoparticles (samples A′, B′, C′, and D′).

Sample	At. Wt.% of Mn found by AAS	UV–Vis absorption (nm)	Band gap E_g (eV)	Particle size (nm)
A′	0.0080	370	3.35	5.42
B′	0.0085	350	3.54	5.18
C′	0.0176	336	3.69	5.02
D′	0.0602	320	3.88	4.83

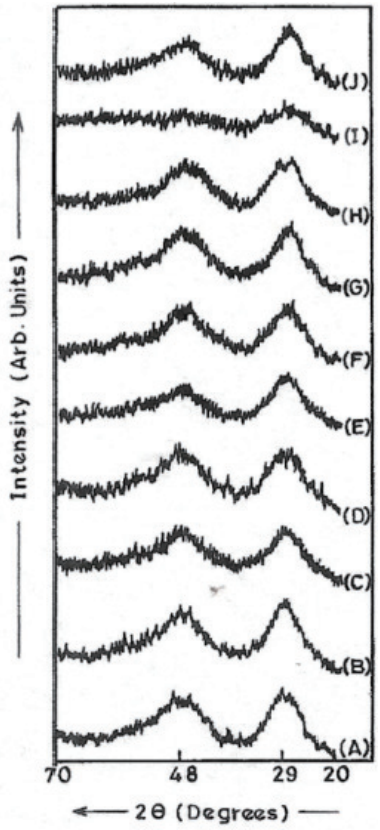

Fig. 8. XRD spectra of Mn-doped CdS nanoparticles (samples A to J).

However, there are reports[22] wherein the composition dependence of the band gap in the case of doping of transition metals, especially Mn with Ⅱ–Ⅵ group semiconductors, is discussed. These reports have demonstrated that the band gap may vary over a large range with Mn composition.

In samples A to J (Fig. 2) and samples A′ to D′ (Fig. 7), there is a decrease in the particle size as the energy gap increases due to higher Mn concentration and in samples R to Z (Fig. 5) there is an increase in the particle size as the energy gap decreases due to lower Mn concentration. This means that the behavior of the particle size and the energy gap depend on the concentration of Mn element in the case of Mn-doped CdS nanoparticles.

A Philips PW 1840 powder X-ray diffractometer with a source of incident radiation, CuKα (λ = 1.542 Å), was used to record the XRD spectra of dry samples. Fig. 8 shows the XRD spectra of Mn-doped CdS nanoparticles (samples A to J) for different atomic weight percentages of Mn element, ranging from 0.068% to 0.154%. These CdS : Mn nanoparticles (having higher Mn concentration) have approximately the same average particle size. The XRD parameters of samples A to J are given in Table 5. Fig. 8 shows that the diffraction patterns are similar for the various Mn concentrations incorporated in CdS nanoparticles. The main peaks of samples A to J at ~29 and ~47 Å referring to the planes (111) and (220) indicate a cubic crystal structure. A cubic crystal structure was also observed in the case of the undoped CdS nanoparticles synthesized in our previous study[33]. The average particle size is found out from the XRD pattern using Scherrer's formula[33, 35]. The average particle sizes of CdS : Mn nanoparticles synthesized in our study are smaller than that calculated by Patel *et al*.[26], Gadalla *et al*.[1], and Venkatesu *et al*.[29].

Fig. 9 shows the emission spectra and the excitation spectra of Mn-doped CdS nanoparticles (samples A to J) recorded at room temperature. The values of excitation and emission wavelengths of those spectra are given in Table 6.

A Perkin Elmer LS–50 fluorescence spectrometer with xenon lamp was used to carry out the PL experiments. PL studies were carried out for samples A to J with various Mn concentrations ranging from 0.068 to 0.154 atomic wt.% at room temperature. The isolated Mn site is mainly responsible for luminescence in samples A to J. Mn^{2+} ions occupy Cd^{2+} lattice sites in the CdS host lattice. In the PL process, an electron from the CdS valence band gets excited across the band gap. The photo excited electron subsequently decays by a nonradiative recombination process to some surface or defect site, or it is captured by Mn^{2+} ions in the $^4T_1$ level, from which it decays radiatively to the $^6A_1$ level. Doping with Mn reduces the probability of nonradiative recombination and causes the CdS to phosphor at about 630 nm (shown in Fig. 1) by a radiative recombination transition between $^4T_1$ and $^6A_1$. The emission with the photon energy of 1.97 eV, by Mn^{2+}, during $^4T_1 \rightarrow {}^6A_1$ transition is quite strong and observable with the naked eye. Bhargava *et al*.[8] proposed in a model that the transition between $^4T_1$ and $^6A_1$ in nanocrystalline Mn-doped ZnS is enhanced due to quantum confinement effects. It has been suggested that the coupling of 3*d* states of Mn ions and *sp* states of ZnS nanoparticles gives rise to a fast transfer of photo excited electrons from the ZnS band to the localized Mn states and the Mn ion derived states, due to the increased overlap of wave functions in nanoparticles. It has been shown that the radiative transition is about five orders of magnitude faster in nanoparticles compared to that in the bulk. The PL is enhanced by surface passivation due to the reduction of available nonradiative recombination centers. Mn-doped superlattices of CdTe and micro crystals of CdS have also been studied by Oka and Yanata[41], who showed their results in terms of quantum confinement and suggested that the luminescence efficiency is enhanced by nanostructures. This has been challenged by Donega *et al*.[42], who concluded from the lifetime measurements and time-resolved spectroscopy that the nanoparticles do not form a new class of luminescent materials because the decay time is not altered from the corresponding bulk material. More experiments may be required to assess the efficiency of nanoparticles as luminescent materials in the future.

The variation of PL intensity with the atomic weight percentage of Mn element has been studied in the PL investigation of samples A to J, which is shown in Fig. 10. From Fig. 10, it can be clearly seen that for lower dopant concentration, the emission peak at 630 nm starts appearing. At an optimum Mn concentration of 0.131 atomic wt.%, the orange emis-

Table 5. XRD parameters of Mn-doped CdS nanoparticles (samples A to J).

Sample	Wt.% of Mn used for chemical reaction	Wt.% of Mn found by AAS	At. Wt.% of Mn found by AAS	XRD average particle size, d' (nm) and inter planar distance, d (Å)	
A	15	3.72	0.068	$2\theta = 29°$ $d' = 5.27$ nm $d = 3.08$ Å	$2\theta = 47.8°$ $d' = 3.72$ nm $d = 1.90$ Å
B	25	4.56	0.083	$2\theta = 28.6°$ $d' = 5.70$ nm $d = 3.12$ Å	$2\theta = 47.7°$ $d' = 3.81$ nm $d = 1.90$ Å
C	35	5.66	0.103	$2\theta = 28.7°$ $d' = 5.33$ nm $d = 3.11$ Å	$2\theta = 47.5°$ $d' = 3.62$ nm $d = 1.91$ Å
D	45	6.48	0.118	$2\theta = 29.2°$ $d' = 4.89$nm $d = 3.05$ Å	$2\theta = 47.6°$ $d' = 4.58$ nm $d = 1.91$ Å
E	50	6.87	0.125	$2\theta = 28.6°$ $d' = 5.19$ nm $d = 3.12$ Å	$2\theta = 47.4°$ $d' = 4.28$ nm $d = 1.92$ Å
F	55	7.20	0.131	$2\theta = 28.8°$ $d' = 4.89$ nm $d = 3.1$ Å	$2\theta = 47.3°$ $d' = 3.56$ nm $d = 1.92$ Å
G	60	7.53	0.137	$2\theta = 28.5°$ $d' = 5.4$ nm $d = 3.13$ Å	$2\theta = 47.5°$ $d' = 3.81$ nm $d = 1.91$ Å
H	65	7.80	0.142	$2\theta = 28.6°$ $d' = 4.94$ nm $d = 3.12$ Å	$2\theta = 47.2°$ $d' = 3.84$ nm $d = 1.92$ Å
I	70	8.02	0.146	$2\theta = 28.8°$ $d' = 3.73$ nm $d = 3.1$ Å	$2\theta = 47.1°$ $d' = 2.83$ nm $d = 1.93$ Å
J	80	8.46	0.154	$2\theta = 28.7°$ $d' = 4.77$ nm $d = 3.11$ Å	$2\theta = 47.7°$ $d' = 3.53$ nm $d = 1.90$ Å

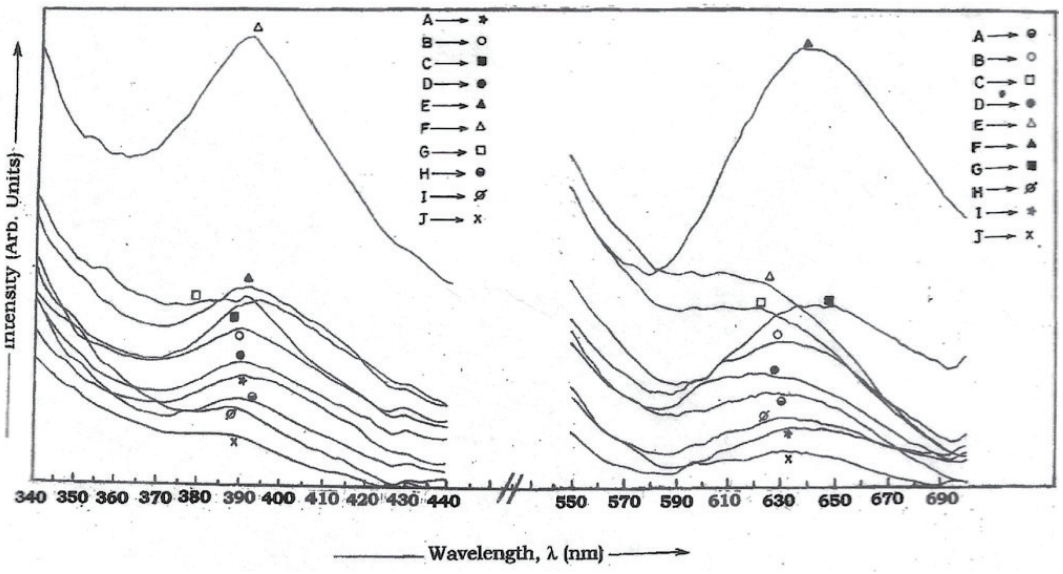

Fig. 9. Excitation and emission spectra of Mn-doped CdS nanoparticles (samples A to J).

sion reaches its maximum intensity. Beyond 0.131 atomic wt.% of Mn, the emission intensity reduces for higher dopant concentration. Thus, it is observed that the quenching of the luminescence intensity[34, 35] occurs in the PL spectrum of CdS : Mn nanoparticles (samples A to J). The excitation wavelength is ~391 nm and the emission wavelength is ~638 nm for maximum PL (sample F). The PL intensity decreased and a red shift was observed in the emission band position with an increase in temperature in the case of Mn^{2+}-doped CdS particles prepared using the sol-gel method by Costa *et al*.[38].

Levy *et al*.[5] recorded the PL spectra of the $Cd_{0.95}Mn_{0.05}S$ nanocrystals with average particle sizes (1.8, 2.8, and 3.2 nm) at room temperature and also at 77 K. The Mn composition was kept constant in these two methods of preparing $Cd_{0.95}Mn_{0.05}S$ nanoclusters. The maximum PL intensity is 570 nm for 1.8 nm sized particles and 700 nm for 3.2 nm sized particles at room temperature. This Mn^{2+} luminescence observed in nanoparticles at room temperature can be attributed to the CdS states of sulfur vacancies and not to the difference in the average particle size. The maximum PL inten-

Table 6. PL parameters of Mn-doped CdS nanoparticles (samples A to J).

Sample	Wt.% of Mn used for chemical reaction	Wt.% of Mn found by AAS	At. Wt.% of Mn found by AAS	PL intensity	
				Excitation λ_{ex} (nm)	Emission λ_{em} (nm)
A	15	3.72	0.068	391.3	625
B	25	4.56	0.083	389.2	626
C	35	5.66	0.103	393.1	628
D	45	6.48	0.118	392.9	631
E	50	6.87	0.125	391.9	634
F	55	7.20	0.131	391.3	638
G	60	7.53	0.137	389	634
H	65	7.80	0.142	387.9	633
I	70	8.02	0.146	389	642
J	80	8.46	0.154	386.1	631

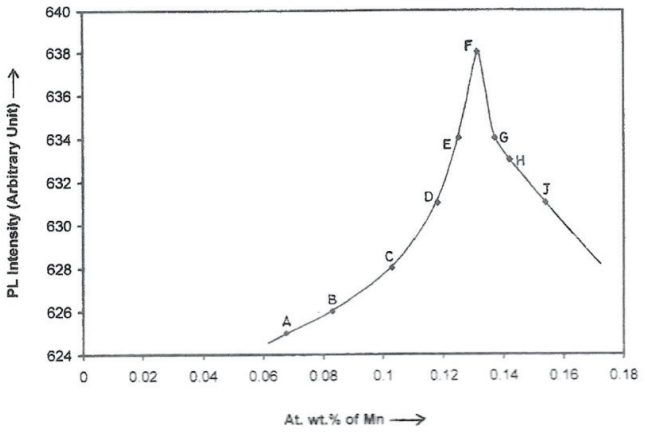

Fig. 10. Variation of PL intensity with atomic weight percentage of Mn in samples A to J.

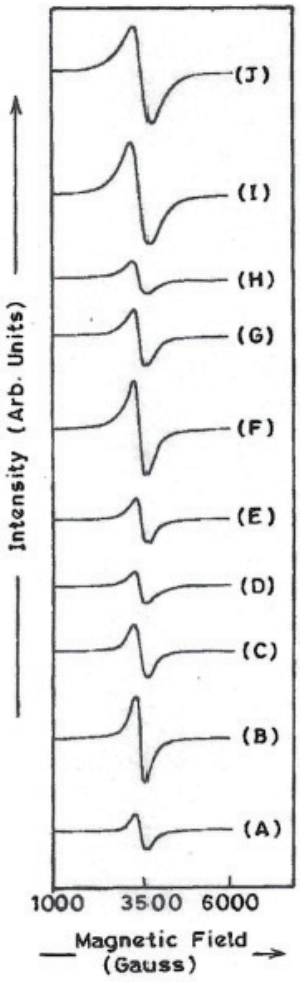

Fig. 11. ESR spectra of Mn-doped CdS nanoparticles (samples A to J).

sities are at 77 K due to Mn^{2+}. There is an increase in the relative quantum yield of fluorescence due to isolated Mn^{2+} with a decrease in temperature. The luminescence intensity due to isolated Mn^{2+} ions varies with the aging or passivation of particles having the similar size. It cannot be attributed to a change in the amount of Mn^{2+} inside the CdS matrix. In addition, the quenching of the luminescence intensity is not observed in $Cd_{0.95}Mn_{0.05}S$ nanoclusters prepared by Levy *et al*.[5].

In our method, the maximum PL intensities were obtained in CdS : Mn nanoparticles (samples A to J) at room temperature. An orange emission is observed at ~630 nm in these nanoparticles due to isolated Mn^{2+} ions. The quenching of the luminescence intensity is also observed in samples A to J having higher Mn concentration. These Mn-doped CdS nanoparticles were prepared by keeping the thioglycerol concentration and the average particle size constant by varying the concentration of Mn element. From Fig. 9, it can be clearly seen that the red shift is observed in the emission wavelength with increasing the Mn concentration.

Mn-doped ZnS nanoparticles of different sizes fluoresce at different wavelengths depending upon the dopant but can be excited with a single wavelength in the UV range[43]. In our case, Mn-doped CdS nanoparticles (samples A to J) of the same average particle size fluoresce at approximately a single wavelength using approximately a single excitation wavelength in the UV range. These nanoparticles can be used as fluorescent objects rather than the conventional fluorophores. Doping CdS nanoparticles with Mn element enhances PL efficiency.

The ESR spectra were recorded for particles with variation of Mn concentration on Bruker EMX-X band spectrometer at room temperature. Fig. 11 shows the ESR spectra of CdS : Mn nanoparticles (samples A to J) doped from 0.068 to 0.154 atomic wt.% of Mn. These nanoparticles have approximately the same averageparticle size. The ESR parameters of samples A to J are given in Table 5. Mn^{2+} has five unpaired 3*d* electrons with total spin $S = 5/2$ and $I = 5/2$[7]. This gives rise to $^6S_{5/2}$ as the ground term. This term splits when it is subjected to a magnetic field. Accordingly, isolated Mn ion at substitutional site in cubic CdS lattice gives rise to a six-line spectrum due to $M_s = 1/2 \rightarrow \pm 1/2$ transitions coupled to Mn nuclear spin. Here, the selection rules are

$$\Delta M_s = \pm 1 \text{ and } \Delta M_I = 0 \quad \text{allowed transitions},$$
$$\Delta M_I = 1 \text{ or } 2 \quad \text{forbidden transitions}. \qquad (3)$$

The ESR spectra of samples A to J (Fig. 11) show that the exchange narrowed signal becomes dominant and dominantly dipolar-broadened spectra are observed due to higher concentration of Mn ions. From these spectra, it is clear that the line width increases and the intensities also vary as the concentration of Mn element increases. The line width increases with the decrease in the average distance between

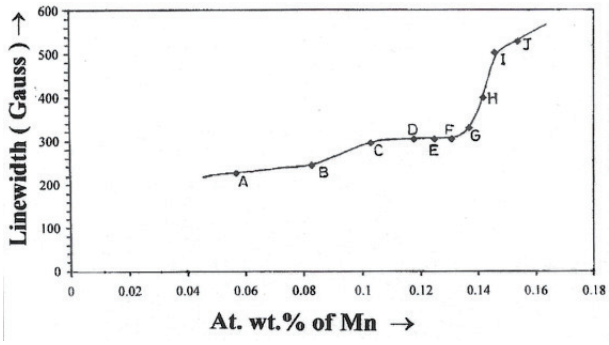

Fig. 12. Variation of line width with atomic weight percentage of Mn (samples A to J).

two Mn ions. Fig. 12 shows the variation of line width with the atomic weight percentage of Mn element in Mn-doped CdS nanoparticles (samples A to J). Similar behavior has been observed by Levy *et al*.[22], who have also recorded the EPR (Electron Paramagnetic Resonance) spectra for particles characterized by the same size (d = 3.2 nm) and for the various Mn compositions. From the EPR spectra shown by Levy *et al*.[22], a drastic broadening of the EPR line width is observed with an increase in Mn composition (Y). The line width strongly decreases by decreasing the Mn composition (Y). This decrease in line width and the linear variation of line width with Y^2 indicate that the Mn ions are randomly distributed and do not form the islets inside a CdS matrix.

Fig. 13 shows the ESR spectra of pure manganese sulphide (MnS) nanoparticles having various molarities of thioglycerol at room temperature. From Fig. 13, it is clearly seen that broadened peaks are observed and the line width remains approximately the same with an increase in concentration of thioglycerol.

The dominantly dipolar-broadened spectra are obtained with an increase in Mn concentration in case of samples A to J (Fig. 11). This means that the line width increases with increasing the Mn concentration. Table 7 shows the ESR parameters of samples A to J. As shown in Table 7, the line width of the sample J is 527.68 Gauss. For pure manganese sulphide, the line width of the broad peak is 628 Gauss. Since the Mn concentration in sample J is less than that in pure manganese sulphide nanoparticles, the line width of sample J is smaller than that of manganese sulphide particles. Levy *et al*.[22] have also shown the same behavior. Levy showed the large EPR spectrum for pure manganese sulphide nanoparticles with a line width equal to 624 Gauss. Levy *et al*. also compared the EPR spectra of CdS : Mn nanoparticles having the various Mn compositions with the EPR spectrum of pure manganese sulphide nanoparticles and stated that the line width strongly decreases by decreasing the Mn composition. Similar behavior has been observed in the bulk phase[22]. This is explained in terms of magnetic interactions between the Mn ions[44]. The dominant anisotropic spin–spin interaction seems to be the anisotropic part of the exchange interaction.

Fig. 14 shows the ESR spectra of CdS : Mn nanoparticles (samples R to Z) doped from 0.0005 to 0.0671 atomic wt.% of Mn having different particle sizes. From these spectra, it can be clearly seen that the line width increases and the average distance between two Mn ions decreases with an increase in Mn concentration. Table 8 shows the ESR parameters of samples R to Z. It can be seen that the samples R to Z show hyperfine splitting due to low concentration of Mn^{2+} ions in CdS. The spectra of samples R to Y are composed of six intense lines and intermediate weaker bands. In sample Z, the six-line spectrum gradually disappears, which indicates that there is exchange interaction between isolated Mn^{2+}–Mn^{2+} ions. Thus, the line width increases with an increase in the Mn concentration in samples R to Z. Each ESR spectrum was analyzed. Fig. 15 shows the variation of line width with the weight percentage of Mn element in Mn-doped CdS nanoparticles (samples R to Z).

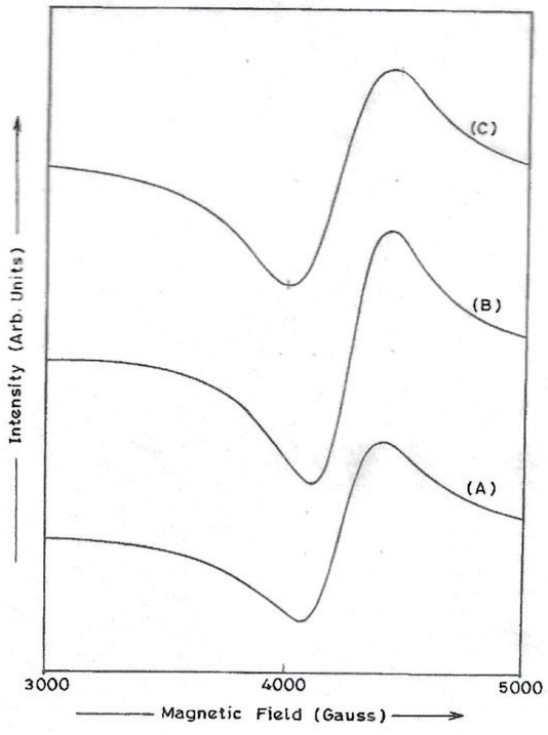

Fig. 13. ESR spectra of manganese sulphide nanoparticles.

Thus, it was possible for us to get the hyperfine splitting for lower Mn concentration and the broad peak for higher Mn concentration at room temperature. The hyperfine interaction between the nuclear spin of the Mn^{2+} ion and the electron depends on the local environment and the location of the Mn element can be determined using the EPR spectra[25]. The values of the g factor and the splitting obtained from the ESR spectrum of sample R (having lower Mn concentration) are equal to 1.9904 and 10 Gauss, respectively. This splitting is smaller than that given in the literature[22] for isolated Mn ions. The values of the g factor and the splitting obtained from the ESR spectrum of sample A (having higher Mn concentration) are equal to 2.0079 and 225.69 Gauss, respectively. The hyperfine structure has been observed by Levy *et al*.[22] at very low Mn composition (Y), but the six resonance lines and the intermediate weaker bands cannot be clearly seen. This structure is due to the extreme weakness of the interaction. This is a characteristic of isolated Mn ions in a tetrahedral site. The g factor is 2.002 and the hyperfine splitting is 70 Gauss, which are obtained from the ESR spectrum. This hyperfine splitting is higher than that obtained in our samples. Our results are in qualitative agreement with the earlier work on Mn-doped CdS nanoparticles prepared using different methods[18, 39].

Table 7. ESR parameters of Mn-doped CdS nanoparticles (samples A to J).

Sample	At. Wt.% of Mn	Line width (Gauss)	Spectroscopic splitting factor (*g*)	B_r[a] (Gauss)	ESR intensity ($\times 10^5$)	ESR intensity/gain	No. of CdS molecules	No. of Mn atoms
A	0.068	225.69	2.0079	3465.8418	1.9101743	1.9101743	6909	1008
B	0.083	243.05	2.0079	3462.2744	4.7703872	1.1925968	4078	628
C	0.103	294.11	2.0128	3457.3715	4.4982699	4.4982699	8038	1053
D	0.118	302.76	2.0077	3466.022	2.7958911	2.7958911	4754	561
E	0.125	302.76	2.0077	3466.022	3.7125768	3.7125768	1998	250
F	0.131	302.76	2.0178	3445.1535	8.6626791	5.4141	6582	934
G	0.137	328.71	2.0178	3448.7209	5.6189461	3.5118413	6625	908
H	0.142	397.92	2.0178	3448.7209	5.0669891	5.0669891	3897	401
I	0.146	501.73	2.0028	3474.6725	2.4355177	19.4841	5231	434
J	0.154	527.68	1.9854	3504.9493	2.561721	16.010756	5384	307

a: B_r is the magnetic field at the center of the two resonance lines.

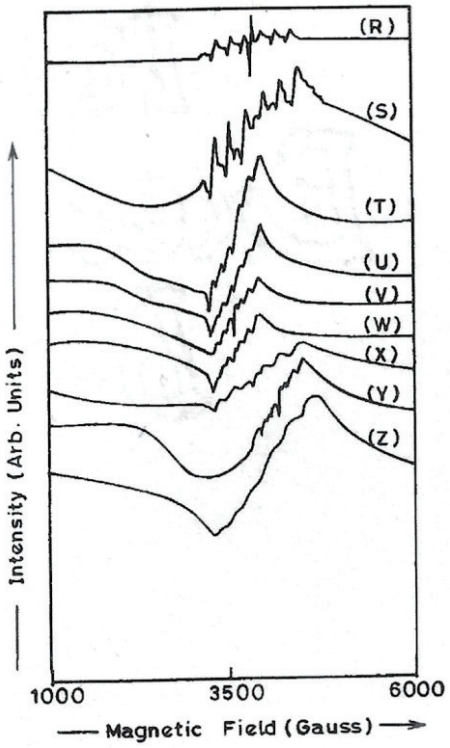

Fig. 14. ESR spectra of Mn-doped CdS nanoparticles (samples R to Z).

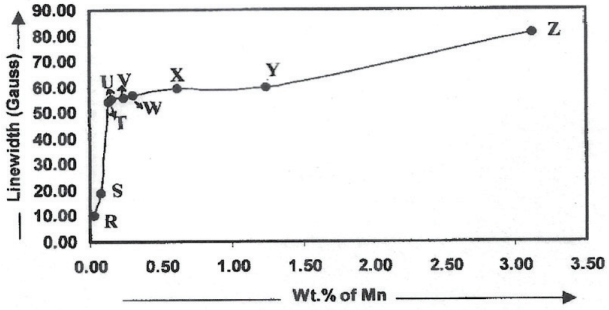

Fig. 15. Variation of line width with weight percentage of Mn in samples R to Z.

Table 8. ESR parameters of Mn-doped CdS nanoparticles (samples R to Z).

Sample	At. Wt.% of Mn found by AAS	Spectroscopic splitting factor (*g*)	Line width (Gauss)
R	0.0005	1.9904	10
S	0.0014	1.9904	19.16
T	0.0024	1.9910	54.17
U	0.0028	1.9902	55
V	0.0044	1.9902	55.87
W	0.0055	1.9902	56.7
X	0.0113	1.9910	59.2
Y	0.0226	1.9909	60
Z	0.0671	1.9904	80.8

Hyperfine splitting was observed in Mn^{2+} doped CdS nanocrystals (1.2 to 2.4 nm in diameter) that were dispersed in organic-inorganic silica xerogels by Counio *et al.*[7] at room temperature and also at 4.2 K. These nanoparticles are prepared by combining a controlled precipitation of nanocrystals in inverted micelles, a separation as a pure capped cluster powder, and dispersion in hydrolyzed silicon alkoxide. The method of preparation of CdS : Mn nanoparticles is different and the ESR spectra are also recorded in a different way in comparison with our method.

The ESR spectra of four more samples A′, B′, C′, and D′ are shown in Fig. 16. These samples show the dominantly dipolar-broadened spectra due to very high Mn concentration. It can be noticed from these ESR spectra that the line width increases as the concentration of Mn element increases. There is a decrease in the average distance between two Mn ions. Fig. 17 shows the variation of line width with the atomic weight percentage of Mn element in Mn-doped CdS nanoparticles (samples A′, B′ C′ and D′). Table 9 shows the comparison between the ESR results obtained in the case of samples A′, B′, C′, and D′.

For the quantum design, an MPMS2-SQUID magnetometer has been used to measure the magnetic properties of two $Cd_{1-x}Mn_xS$ (the concentration of Mn ions, $x = 0.04, 0.05$) samples. A magnetic field ranging between +1 and −1 Tesla was applied to these samples to measure the magnetization as a function of the applied magnetic field at 300 and 5 K. These $Cd_{1-x}Mn_xS$ samples showed a ferromagnetic ordering at all temperatures ranging from 5 to 300 K and their $M(H)$ curves consist of ferromagnetic and paramagnetic terms.

Fig. 18 shows the $M(H)$ loops (hysteresis loops) of two $Cd_{1-x}Mn_xS$ powder samples ($x = 0.04, 0.05$) at 300 K after subtracting the paramagnetic contributions. The hysteresis curves observed in Fig. 18 show the variation of the magnetic induction or intensity of magnetization M with the magnetizing field (H) by keeping the temperature constant. In

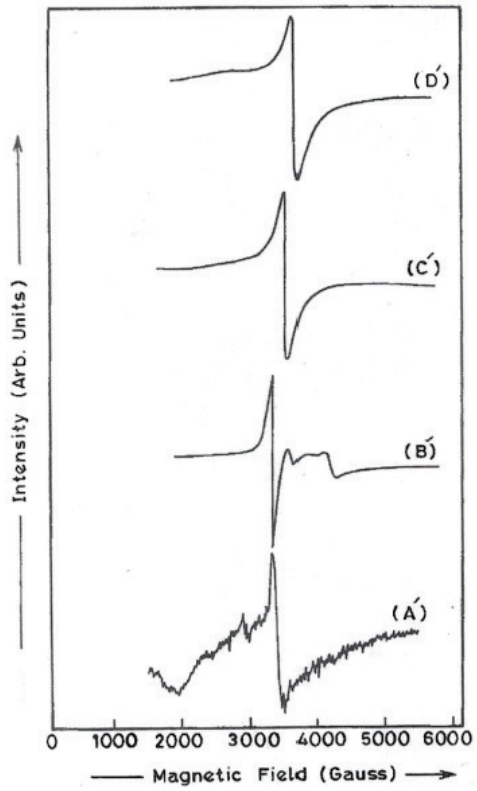

Fig. 16. ESR spectra of Mn-doped CdS nanoparticles (samples A′, B′, C′ and D′).

case of sample $Cd_{1-x}Mn_xS$ (x = 0.04), the intensity of magnetization M remains constant if the magnetic field is increased above 2500 Oe. At this stage, this sample becomes saturated. In the case of sample $Cd_{1-x}Mn_xS$ (x = 0.05), the intensity of magnetization M does not become constant, even if the magnetic field is increased above 2500 Oe, but keeps on increasing at a low rate. Therefore, the $M(H)$ curve slopes very slightly upward and after 5000 Oe the sample $Cd_{1-x}Mn_xS$ (x = 0.05) becomes saturated. Thus, it is concluded that the saturation magnetization (M_s) is higher in 4% Mn-doped CdS than 5% Mn-doped CdS.

From Fig. 18, it can be observed that the remanent magnetism of the sample $Cd_{1-x}Mn_xS$ (x = 0.04) is higher than that of the sample $Cd_{1-x}Mn_xS$ (x = 0.05). Therefore, in the case of sample $Cd_{1-x}Mn_xS$ (x = 0.04), a large coercive force is required to remove the remanent induction. Therefore, it can be said that the sample $Cd_{0.96}Mn_{0.04}S$ is a hard magnetic material as compared to the sample $Cd_{0.95}Mn_{0.05}S$. Mn-doped CdS quantum dots prepared by Maity *et al*.[4] produced a small coercive field which indicates a weak ferromagnetism. The $M(H)$ curves produced in the vibrating sample magnetometry analysis of Mn-doped CdS nanoparticles synthesized in our study are hysteresis curves, but the $M(H)$ curves exhibited by Maity *et al*.[4] are not the hysteresis curves. Similarly, no hysteresis was observed by Venkatesu *et al*.[29, 45]. This indicates that the CdS : Mn nanoparticles prepared by Maity *et al*.[4] and Venkatesu *et al*.[29, 45] are paramagnetic. Those nanoparticles show a weak ferromagnetism at room temperature by the small hysteresis loop[4, 29].

The values of the saturation magnetization M_s, which are obtained at higher magnetizing fields H after subtracting the linear part in $M(H)$ curves, and the corresponding coercivity values, H_c for the two $Cd_{1-x}Mn_xS$ (x = 0.04, 0.05) samples are

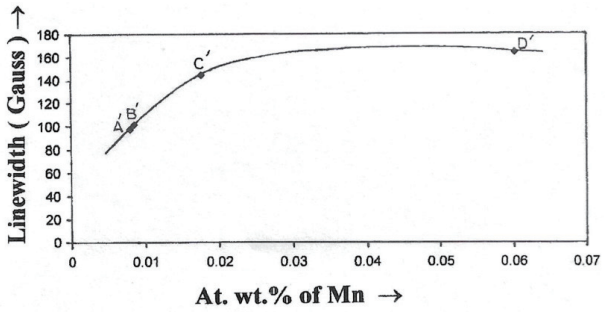

Fig. 17. Variation of line width with atomic weight percentage of Mn in samples A′, B′, C′, and D′.

given in Table 10. From Table 10, it can be observed that the M_s values are decreasing with increasing the temperatures in both of the samples.

Fig. 19 shows that the magnetization intensity or magnetic induction M varies with the temperature by keeping the magnetizing field H constant at 1 KOe for the sample $Cd_{0.96}Mn_{0.04}S$. This sample is a composite of ferromagnetic and paramagnetic contributions. A dominant linear variation of magnetic induction is observed at low temperature, whereas at higher temperatures the magnetic induction gradually varies with temperature and after 200 K it becomes constant. The contribution is largely ferromagnetic at higher temperatures and the intensity of magnetization follows the classical Bloch law for low lying spin wave excitations: $M(T) = M(0)(1 - AT^{3/2})$[46]. The saturation magnetization obtained from the curve is 4.91×10^{-3} emu/g and the stiffness coefficient is 7×10^{-5} $K^{-3/2}$.

The magnetic susceptibility of ferromagnetic substance decreases with the temperature and obeys Curie's law, which is expressed as

$$X \propto \frac{1}{T}, \tag{4}$$

$$X \times T = \text{constant}. \tag{5}$$

At a critical temperature or Curie point T_c, the value of magnetic susceptibility drops suddenly and the body becomes paramagnetic. The susceptibility X of a ferromagnetic substance above its Curie point is inversely proportional to the difference of temperature of the substance and the Curie point, i.e., X, varies as $\frac{C}{T - T_c}$, where C is the Curie constant. This is the Curie–Weiss law.

Fig. 20 shows the variation of the energy difference per unit cell between the ferromagnetic (FM) and anti-ferromagnetic (AFM) alignments of the two Mn spins $\Delta E_{FM\text{-}AFM}$ (meV) with the concentration of the Mn element (%). Ferromagnetism is an ability to sustain magnetization even in zero applied magnetic field below the Curie temperature T_c. The ferromagnetic materials can be magnetized to a great extent. Most of their individual magnetic moments can be aligned parallel to each other. In the ferromagnetic materials, the magnetization is not clearly proportional to the magnetizing force. Therefore, the susceptibility varies considerably with the magnetizing force and it also varies with the temperature in ferromagnetic materials. In anti-ferromagnetic materials, the magnetic moments on alternate (or neighboring) lattice sites are

Table 9. ESR parameters of Mn-doped CdS nanoparticles (samples A′, B′, C′, and D′).

Sample	Wt.% of Mn found by AAS	At. Wt.% of Mn found by AAS	Line width (Gauss)	B_r (Gauss)	ESR intensity ($\times 10^5$)	Spectroscopic splitting factor (g)
A′	0.439	0.0080	97.7	3370.5	0.1055	2.068
B′	0.469	0.0085	101.7	2535.7	2.5	2.050
C′	0.969	0.0176	144.7	3374.4	0.955	2.066
D′	3.309	0.0602	164.2	3384.2	1.087	2.060

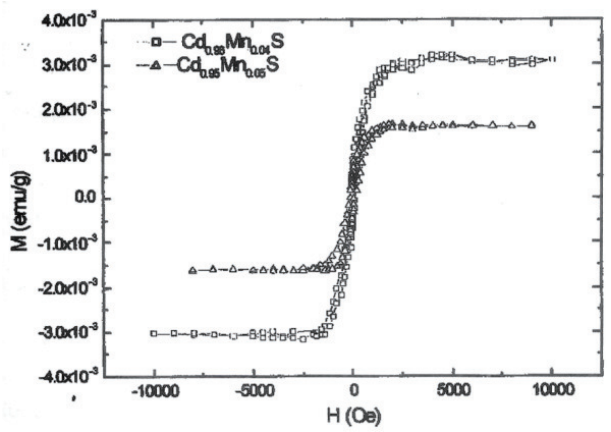

Fig. 18. $M(H)$ curves of two $Cd_{1-x}Mn_xS$ samples (x = 0.04, 0.05) at 300 K.

Table 10. VSM parameters of two $Cd_{1-x}Mn_xS$ powder samples (x = 0.04, 0.05).

Sample	M_s at 300 K (emu/g)	M_s at 5 K (emu/g)	H_c at 300 K (Oe)	H_c at 5 K (Oe)
$Cd_{0.95}Mn_{0.05}S$	$\sim 1.61 \times 10^{-3}$	$\sim 1.59 \times 10^{-2}$	~105	~250
$Cd_{0.96}Mn_{0.04}S$	$\sim 3.07 \times 10^{-3}$	$\sim 3.84 \times 10^{-2}$	~100	~98

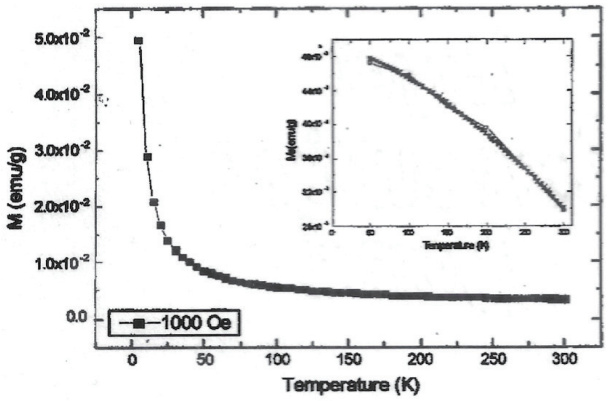

Fig. 19. Temperature dependence of magnetization for $Cd_{0.96}Mn_{0.04}S$ at 1 KOe. The inset shows the best fit to the Bloch law $M(T) = M(0) \times (1 - AT^{3/2})$ (shown by the marked line).

aligned antiparallel to each other. Therefore, in these materials no net magnetization is present. This type of magnetic order also occurs spontaneously in certain materials below a specific temperature, which is called the Neel temperature T_N. Above T_N, this material also becomes paramagnetic. Whether a material will become ferromagnetic or anti-ferromagnetic below a certain temperature depends upon the magnetic exchange interactions between the neighboring ions.

In short configuration, the two Mn atoms are separated by a single S atom whereas in the far configuration, the two Mn atoms are separated by two S atoms. Fig. 20 shows that the short configuration is higher in energy than the far configuration. The AFM behavior can be observed for all of the Mn concentrations in the short configuration. The energy difference between the ferromagnetic (FM) and the anti-ferromagnetic (AFM) states remains almost constant (approximately 15 meV) for Mn concentration values between 0.056 and 0.021. These results agree with the experimental results obtained from Fig. 19, which do not show ferromagnetism at low temperatures (below 5 K). The paramagnetic behavior observed at temperatures less than 5 K has also been reported by the other researchers[19, 47]. Fig. 19 shows the ferromagnetic behavior of Mn-doped CdS nanoparticles at higher temperatures. However, it can be seen from from Fig. 20 that the ferromagnetic configuration is not the energetically most stable one for all the given concentrations of Mn element.

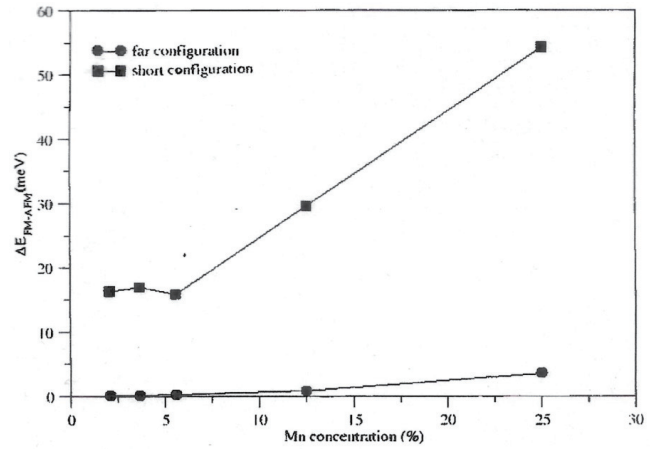

Fig. 20. Total energy difference $\Delta E_{FM\text{-}AFM}$ between ferromagnetic and anti-ferromagnetic configurations for Mn-doped CdS nanoparticles as a function of Mn concentration in the "short" (squares) and "far" (circles) configurations.

Fig. 21 shows a transmission electron microscopy (TEM) image and the selected area electron diffraction (SAED) pattern of Mn-doped CdS nanoparticles (sample A) having large particle size due to the lower concentration of Mn element. The large clusters of the size 181.5 nm having the spherical shape are observed in sample A.

Fig. 22 shows a TEM image and the SAED pattern of Mn-doped CdS nanoparticles (sample J) having small particle size due to the higher concentration of Mn element. Small clusters of size 36.6 nm with a spherical shape are observed in sample J. It was possible to observe sphere shaped CdS : Mn particles having the various sizes with high magnification. The ring patterns observed in the SAED images of samples A and J show the polycrystalline nature of CdS : Mn nanoparticles. The indexed planes (111), (220) shown by the rings, belong to the cubic structure and are consistent with the XRD results of samples A and J. Similar SAED patterns were observed in case of Mn-doped CdS nanoparticles prepared by Patel *et al.* using the chemical co-precipitation method[26]. The size and

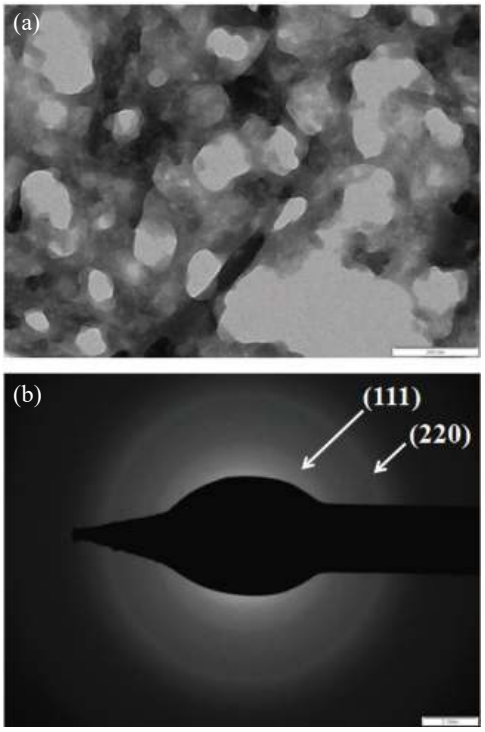

Fig. 21. (a) TEM image of Mn-doped CdS nanoparticles (sample A) with magnification of 200 nm and (b) SAED pattern of Mn-doped CdS nanoparticles (sample A).

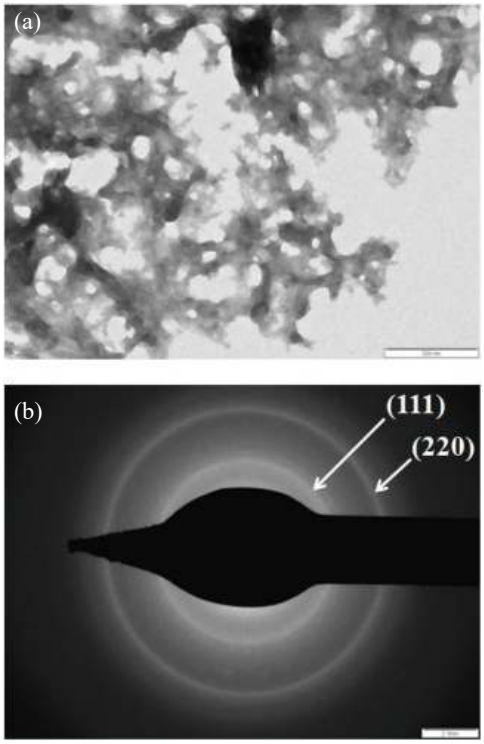

Fig. 22. (a) TEM image of Mn-doped CdS nanoparticles (sample J) with magnification of 200 nm and (b) SAED pattern of Mn-doped CdS nanoparticles (sample J).

the shape of CdS : Mn nanoparticles (samples A and J) remain unchanged even after doping of CdS nanoparticles with the Mn element. This Mn doping produces the coalescence of particles, which depends on the Mn concentration. The TEM results obtained in our study are in agreement with the TEM results observed by Patel *et al*.[26].

4. Conclusions

It was possible to dope CdS nanoparticles with Mn element by a very simple and inexpensive method. CdS nanoparticles with narrow size distribution are synthesized by the non-aqueous chemical method. Thioglycerol has been used as the capping agent. The conclusions obtained from the investigations of Mn-doped CdS nanoparticles done by using the various characterization techniques are given below.

The quantum size effect is observed in Mn-doped CdS nanoparticles. The appearance of the orange emission at wavelength ~630 nm can be seen due to $^4T_1 \rightarrow {}^6A_1$ transition. The isolated Mn site is mainly responsible for luminescence in CdS : Mn nanoparticles. The quenching of PL intensity is also observed in CdS : Mn nanoparticles. The concentration of Mn element is responsible for luminescence quenching in doped particles. The CdS quantum particles could be doped with Mn element at room temperature with different Mn concentrations, resulting in intense luminescence peaks of orange emission observable by the naked eyes. The Mn concentration variation in different samples has been studied by AAS. The small amount of Mn has a decisive role in luminescence properties of doped CdS particles. These nanoparticles show the hyperfine splitting due to Mn^{2+} ions for lower Mn concentration and the broad peak for higher Mn concentration at room temperature. Mn-doped CdS nanoparticles have been studied. These nanoparticles show ferromagnetism at room temperature. The XRD analysis shows a cubic structure of the doped nanoparticles. The uniformity (without defects) of the spherical clusters was shown by the TEM images. The polycrystalline nature and the indexed planes indicating the cubic phase of the doped nanoparticles were shown by the SAED patterns. These CdS : Mn nanoparticles have potential applications in photovoltaics, optics, nonlinear optics, and photocatalysis.

The research of doped nanoparticles is a topic of tremendous interest. The doped nanoparticles are considered as better phosphor materials due to their peculiar properties and industrial importance. For this, more detailed studies on the aspects like luminescence efficiency, decay time, and so on are required. The size and shape dependence of small particles is an interesting topic that needs to be investigated in more detail. The effect of quantum confinement on *g*-value will also be of deep interest in ESR studies of CdS : Mn nanoparticles. These nanoparticles will lead to better devices, such as LEDs, rectifying diodes, spintronics, electroluminescent devices, and so on.

Acknowledgements

We would like to thank the Head of the Physics Department and the Head of the Chemistry Department of Savitribai Phule Pune University for extending their cooperation and making the facilities of the department available to us for our work. Our sincere and heartfelt thanks to the Head of the Chemistry Department of Savitribai Phule Pune University for allowing us to operate the UV–Vis Absorption and PL instruments.

We are thankful to the SEM, EDX, Mapping, and XRD operators of the Chemistry Department of Savitribai Phule Pune University for their technical support and help provided during

SEM, EDX, Mapping, and XRD characterizations. We are also grateful to the AFM operator of Physics Department of Savitribai Phule Pune University for AFM characterization.

We are thankful to the TEM operator and the operator carrying out the measurements of the thin film thickness from IIT Powai, Mumbai for providing us the TEM and thin film thickness measurement facilities, respectively.

References

[1] Gadalla A, Almokhtar M, Abouelkhir A N. Effect of Mn doping on structural, optical and magnetic properties of CdS diluted magnetic semiconductor nanoparticles. Chalcogenide Letters, 2018, 15, 207

[2] Chaure S. Investigation of the effect of manganese doping in CdS nanocrystalline thin films. Mater Res Express, 2018, 6, 025912

[3] Venkatesan D, Deepan D, Ramkumar J, et al. Synthesis and characterization of sodium bis (2-ethylhexyl) sulfonsuccinate (AOT) capped pure and Mn-doped CdS nanoparticles. J Nanomater, 2012, 2012, 1

[4] Maity P, Kumar R, Jha S N, et al. Investigation of the Physical Properties of Mn-doped CdS Diluted Magnetic Semiconductor Quantum Dots: Non-linear Band Gap variation with Downwards Bowing. Available at SSRN 4066164

[5] Levy L, Ingert D, Feltin N, et al. $Cd_{1-y}Mn_yS$ nanoparticles: Absorption and photoluminescence properties. J Cryst Growth, 1998, 184/185, 377

[6] Hofmann D M, Hofstaetter A, Leib U, et al. EPR and ENDOR investigations on CdS : Mn nanocrystals. J Cryst Growth, 1998, 184/185, 383

[7] Counio G, Esnouf S, Gacoin T, et al. CdS : Mn nanocrystals in transparent xerogel matrices: synthesis and luminescence properties. J Phys Chem, 1996, 100, 20021

[8] Bhargava R N, Gallagher D, Hong X, et al. Optical properties of manganese-doped nanocrystals of ZnS. Phys Rev Lett, 1994, 72, 416

[9] Khosravi A A, Kundu M, Jatwa L, et al. Green luminescence from copper doped zinc sulphide quantum particles. Appl Phys Lett, 1995, 67, 2702

[10] Khosravi A A, Kundu M, Kuruvilla B A, et al. Manganese doped zinc sulphide nanoparticles by aqueous method. Appl Phys Lett, 1995, 67, 2506

[11] Bhargava R N, Gallagher D, Welker T, et al. Doped nanocrystals of semiconductors - a new class of luminescent materials. J Lumin, 1994, 60/61, 275

[12] Bhargava R N. Nanoparticles and their use for multifunctional bioimaging. J Lumin, 1996, 70, 85

[13] Norris D J, Yao N, Charnock F T, et al. High-quality manganese-doped ZnSe nanocrystals. Nano Lett, 2001, 1, 3

[14] Ochsenbein S T, Gamelin D R. Quantum oscillations in magnetically doped colloidal nanocrystals. Nat Nanotechnol, 2011, 6, 112

[15] Beaulac R, Ochsenbein S, Gamelin D, et al. Colloidal transition-metal-doped quantum dots. In nanocrystal quantum dots. CRC Press, 2010, 397

[16] Yu J H, Liu X Y, Kweon K E, et al. Giant Zeeman splitting in nucleation-controlled doped CdSe : Mn^{2+} quantum nanoribbons. Nat Mater, 2010, 9, 47

[17] Wood V, Halpert J E, Panzer M J, et al. Alternating Current driven electroluminescence from ZnSe/ZnS : Mn/ZnS nanocrystals. Nano Lett, 2009, 9, 2367

[18] Levy L, Feltin N, Ingert D, et al. Three dimensionally diluted magnetic semiconductor clusters $Cd_{1-y}Mn_yS$ with a range of sizes and compositions: dependence of spectroscopic properties on the synthesis mode. J Phys Chem B, 1997, 101, 9153

[19] Liu S M, Liu F Q, Guo H Q, et al. Surface states induced photoluminescence from Mn^{2+} doped CdS nanoparticles. Solid State Commun, 2000, 115, 615

[20] McClure D S. Electronic spectra of molecules and ions in crystals part II. Solid State Physics, 1959, 9, 399

[21] Tanabe Y, Sugano S. On the absorption spectra of complex ions I, II. J Phys Soc Jpn, 1954, 9, 753

[22] Levy L, Hochepied J F, Pileni M P. Control of the size and composition of three dimensionally diluted magnetic semiconductor clusters. J Phys Chem, 1996, 100, 18322

[23] Romčević N, Kostic R, Romčević M, et al. Raman spectroscopy of $Cd_{1-x}Mn_xS$ quantum dots. J Phys D: Appl Phys, 2005, 38, 4321

[24] Patle U S, Ahirwar R K, Bhatt A, et al. Enhanced photoluminescence properties of Mn doped CdS nanocrystals. AIP Conf Proc, 2019, 2100, 020165-1

[25] Babi Stoji B, Milivojevi D, Comor M, et al. Optical and electron paramagnetic resonance spectroscopy of $Cd_{1-x}Mn_xS$ quantum dots. J Phys: Condens Matter, 2004, 16, 4625

[26] Patel N H, Deshpande M P, Bhatt S V, et al. Structural and magnetic properties of undoped and Mn doped CdS nanoparticles prepared by chemical co-precipitation method. Adv Mater Lett, 2014, 5, 671

[27] Chauhan R, Kumar A, Chaudhary R P. Synthesis, structural and photocatalytic studies of Mn-doped CdS nanoparticles. Res Chem Intermed, 2013, 39, 645

[28] Gadalla A A, Aboelkhir A N, Mahesha M G, et al. RETRACTED ARTICLE**:** Synthesis and characterization of Mn-doped CdS-diluted magnetic semiconductor nanoparticles. J Mater Sci: Mater Electron, 2020, 31, 10941

[29] Venkatesu P. Doping effect of Mn on structural optical magnetic and electrical properties of CdS nanoparticles. International Conference on Advanced Nanomaterials & Emerging Engineering Technologies, 2013, 260

[30] Malik M A, O' Brien P, Revaprasadu N. Synthesis of TOPO-capped Mn-doped ZnS and CdS quantum dots. J Mater Chem, 2001, 11, 2382

[31] Keerthana S, Yuvakkumar R, Ravi G, et al. PVP influence on Mn-CdS for efficient photocatalytic activity. Chemosphere, 2021, 277, 130346

[32] Patle U S. Synthesis and characterization of Mn doped CdS nanoparticles prepared by chemical bath deposition method. International Journal of Science and Research (IJSR), 2015, 4, 1945

[33] Darekar M S, Praveen B M. Synthesis and characterization of nanoparticles of semiconducting metal suplhide and their application. Phys Scr, 2022, 97, 065805

[34] Darekar M S, Praveen B M. High photosensitivity nanocrystalline p-Cu_2S/n-FTO heterojunction photodetectors prepared by dip coating method. J Mod Nanotechnol, 2023, 3

[35] Dareka M S, Praveen B M. Effects of heat treatment in air atmosphere on dip coating deposited CdS thin films for photo sensor applications. J Mod Nanotechnol, 2023, 3

[36] Ikeda M, Itoh K, Sato H. Electrical and optical properties of CdS-MnS single crystals. J Phys Soc Jpn, 1968, 25, 455

[37] Tsai C T, Chen S H, Chuu D S, et al. Fabrication and physical properties of radio frequency sputtered $Cd_{1-x}Mn_xS$ thin films. Phys Rev B, 1996, 54, 11555

[38] Costa V C, Shen Y R, Bray K L. Luminescence properties of nanocrystalline CdS and CdS : Mn^{2+} doped silica-type glasses. J Non Cryst Solids, 2002, 304, 217

[39] Hoffman D M, Meyer B K, Ekimov A I, et al. Giant internal magnetic fields in Mn doped nanocrystal quantum dots. Solid State Commun, 2000, 114, 547

[40] Zhang Y N, Raman N, Bailey J K, et al. A new sol-gel route for the preparation of nanometer-scale semiconductor particles that exhibit quantum optical behavior. J Phys Chem, 1992, 96, 9098

[41] Oka Y, Yanata K. Excitonic properties of nanostructure semimagnetic semiconductors. J Lumin, 1996, 70, 35

[42] de Mello Donegá C, Bol A A, Meijerink A. Time-resolved luminescence of ZnS : Mn^{2+} nanocrystals. J Lumin, 2002, 96, 87
[43] Ethiraj A S, Hebalkar N, Kulkarni S K, et al. Enhancement of photoluminescence in manganese-doped ZnS nanoparticles due to a silica shell. J Chem Phys, 2003, 118, 8945
[44] Samarth N, Furdyna J K. Electron paramagnetic resonance in $Cd_{1-x}Mn_xS$, $Cd_{1-x}Mn_xSe$, and $Cd_{1-x}Mn_xTe$. Phys Rev B Condens Matter, 1988, 37, 9227
[45] Venkatesu P, Ravichandran K. Manganese doped cadmium sulphide (CdS : Mn) quantum particles: Topological, photoluminescence and magnetic studies. Adv Mater Lett, 2013, 4, 202
[46] Maaz K, Karim S, Lee K J, et al. Effect of temperature on the magnetic characteristics of $Ni_{0.5}Co_{0.5}Fe_2O_4$ nanoparticles. Mater Chem Phys, 2012, 133, 1006
[47] Feltin N, Levy L, Ingert D, et al. Magnetic properties of 4-nm $Cd_{1-y}Mn_yS$ nanoparticles differing by their compositions, *y*. J Phys Chem B, 1999, 103, 4

Madhavi Sharad Darekar received her Ph.D. (Physics) in the field of synthesis and characterization of undoped and doped semiconductor nanoparticles from the Department of Physics, Savitribai Phule Pune University, India, in 2006. She received a Post-Doctoral Fellow degree in Nanotechnology from the Department of Nanotechnology, Srinivas University, India, in 2023. At present, she is pursuing a Post-Doctoral Fellow course in Physics in the Department of Physics, Srinivas University, India. Her research involves synthesis of undoped and doped semiconductor nanoparticles by chemical method, thin film deposition by spin coating method, dip coating method, chemical bath deposition etc., their characterizations and applications.